Class of diatomic ferroelectrics with multifunctional properties: IV-VI compounds in the distorted NiAs-type structure

Hu Zhang,[1,2] Bei Deng,[1] Wei-Chao Wang,[2] and Xing-Qiang Shi[1,*]

[1]*Department of Physics, South University of Science and Technology of China, Shenzhen 518055, China*

[2]*Department of Electronics and Tianjin Key Laboratory of Photo-Electronic Thin Film Device and Technology, Nankai University, Tianjin 300071, China*

(Received 9 July 2017; revised manuscript received 11 December 2017; published 26 December 2017)

Ferroelectrics have attracted a great deal of attention, but diatomic ferroelectrics are less common. Here we establish a class of diatomic ferroelectrics in the *distorted* NiAs-type structure based on state-of-the-art first-principles calculations. These compounds, with giant Rashba effect, possess rich phases, ranging from ferroelectric semiconductors to ferroelectric semimetals. Topological surface states and type-II bulk Dirac fermions are found in the *undistorted* phases. This class of multifunctional materials has potential applications in spin-orbitronics.

DOI: 10.1103/PhysRevB.96.245136

I. INTRODUCTION

A ferroelectric is typified as a polar system with a spontaneous electric polarization that can be switched readily by an external electric field. The ferroelectric phase can be obtained from a symmetry-breaking distortion of a nonpolar high-symmetry reference state [1,2]. Apart from the fundamental interest, ferroelectrics also have important technological applications, including nonvolatile memories and electromechanical devices [3,4], etc. Ever since the recognition of ferroelectricity in Rochelle salt [5], many materials were identified to be ferroelectrics. To our knowledge, the most common category of ferroelectrics has perovskites structure ABX_3, in which both A and B are cations, while X is an anion. Consider for example, $BaTiO_3$, the extensive investigations on this perovskite oxide have largely promoted the understanding of ferroelectricity in the past few decades. In 2012, a class of ternary ferroelectrics, in a form of *ABC* compounds in the LiGaGe structure, was predicted based on first-principles studies [6]. Very recently, two-dimensional ferroelectric materials were also predicted from first-principles [7–12].

The amount of known diatomic bulk ferroelectrics is very limited up to now. GeTe, with $R3m$ symmetry, is a well-known diatomic ferroelectric typified with a narrow band gap, which is obtained from the distortion of the cubic rocksalt structure along the [111] direction [13,14]. Crystals in wurtzite-structure (e.g., ZnO) with a polar space group $P6_3mc$ are generally not considered as ferroelectrics since the switch of the polarization cannot be achieved experimentally, due to the difficulty in breaking the strong sp^3 bonding upon the switch [2,6]. The design of diatomic ferroelectrics with a simple crystal structure not only extends the amount of diatomic ferroelectrics thereby further promoting the understanding of ferroelectricity, but also provides us with materials for applications of high-performance devices, with tunable properties on the basis of giant Rashba effect.

In this paper, based on first-principles calculations we identify a class of diatomic ferroelectrics in the distorted NiAs-type structure (space group $P6_3mc$). The NiAs-type structure is a well-known simple crystal structure but has never been associated with ferroelectricity. We first take lead chalcogenides PbX (X = S, Se, and Te) as examples to study this class of potential ferroelectrics, and then we generalize the discussions to other lead-free IV-VI compounds and also other compounds in the NiAs-type structure. The nonpolar high-symmetry paraelectric phase is in the undistorted NiAs-type structure with space group $P6_3/mmc$, as typified in Fig. 1(a). A transverse optic (TO) mode in the high-symmetry phase, with an imaginary frequency at the Brillouin zone (BZ) center, is able to effectively drive the polar distortion. Red arrows in Fig. 1(d) indicate the distortion of the anion relative to the cation. This polar distortion is largely correlated with the *active* lone pair [15] in the group IV cations of compounds in the distorted NiAs-type structure. In addition to semiconducting ferroelectrics, we also report semimetallic ferroelectrics in polar phases of PbTe, SnTe, and GeTe, etc. Although ferroelectric-like structural transitions in metals have been predicted may years ago [16], a ferroelectric metal $LiOsO_3$ was only recently confirmed experimentally [17]. Apart from ferroelectricity, relativistic phenomena including giant Rashba effects and topological surface states are also found in these compounds. Rashba effects appear in polar bulk materials with strong spin-orbit coupling (SOC), in which the spin degrees of freedom can be controlled via the reversal of the ferroelectric polarization by an electric field. Rashba ferroelectrics can be used to design, for example, Datta-Das spin transistor [18,19]. Our calculations indicate that nonpolar PbSe has topological surface states protected by time-reversal (TR) symmetry [20–22]. What's more interesting, we discover that type-II bulk Dirac fermions [23–26] could exist in nonpolar PbTe. The above-mentioned multifunctional characters of these compounds discovered in our current work make them suitable for spin-orbitronics applications [27].

II. METHODOLOGY

We performed first-principles calculations based on density functional theory (DFT) [28] with the Perdew–Burke–Ernzerhoff (PBE) functional in generalized gradient approximation (GGA) [29] as implemented in the Vienna *ab initio*

*shixq@sustc.edu.cn

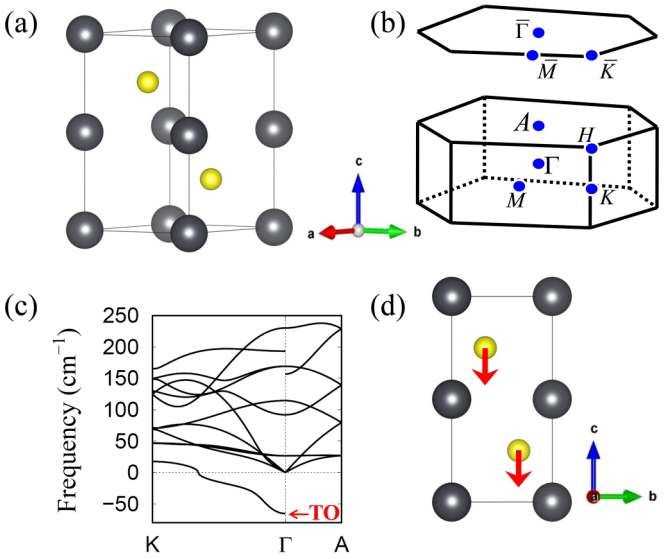

FIG. 1. (a) The atomic structures of nonpolar high-symmetry structures in the NiAs-type structure ($P6_3/mmc$). (b) Brillouin zone of bulk and the projected surface Brillouin zone of (0001) planes. (c) Phonon spectrum (imaginary frequencies are indicated as negative values) of nonpolar high-symmetry PbS. (d) Side view of the high-symmetry structure. Red arrows indicate the displacements of the anion relative to the cation.

simulation package (VASP) [30–32]. The atomic structures were relaxed until the Hellmann-Feynman forces are less than 1 meV/Å. An energy cutoff of 500 eV and a $8 \times 8 \times 8$ Monkhorst-Pack grid [33] were used. We calculated the polarization with the Berry phase method [34]. The phonon spectra were calculated with phonopy [35]. The Heyd-Scuseria-Ernzerhof (HSE) hybrid functional [36] was used to check the band structure of nonpolar PbSe.

To further study the physical properties of the nonpolar high-symmetry PbSe ($P6_3/mmc$), we constructed an effective low energy tight-binding model with the maximally localized Wannier functions with a basis of Pb $6s, 6p$ and Se $4s, 4p$ orbitals using Wannier90 package [37,38]. The Z_2 topological invariants $(\nu_0; \nu_1, \nu_2, \nu_3)$ can be used to classify topological properties, which are calculated through calculations of Wannier charge centers (WCCs) in six time-reversal-invariant planes in the BZ: $k_x = 0, \pi$, $k_y = 0, \pi$, and $k_z = 0, \pi$ planes. The surface spectrums can be obtained by calculating the surface Green's function for a semi-infinite system using the iterative Green's function method. The obtained tight-binding parameters were used to calculate the Z_2 topological invariants $(\nu_0; \nu_1, \nu_2, \nu_3)$ and the surface spectrums with the software package WannierTools [39].

III. RESULTS AND DISCUSSION

A. Ferroelectric properties

In the nonpolar NiAs-type crystal structure of PbS with the $P6_3/mmc$ symmetry, the Pb atoms are in the Wyckoff position 2a (0, 0, 0) and the S atoms in 2c (1/3, 2/3, 1/4). The calculated lattice constants are $a = 4.15$ Å, $c = 7.35$ Å, in qualitative accordance with the local density approximation (LDA) results ($a = 4.00$ Å, $c = 7.14$ Å) reported in previous investigations [40]. The slight discrepancy here is due to the typical difference in exchange-correlation between GGA and LDA.

TABLE I. Theoretical results for polar PbX (X = S, Se, and Te) in the distorted NiAs-type structure. z_X is the position of X in the z direction. ΔE is the energy difference (calculated with SOC) between the polar state ($P6_3mc$) and the nonpolar state ($P6_3/mmc$).

	a (Å)	c (Å)	z_X	ΔE (meV)
PbS	4.150(4.04[a])	7.561(7.27[a])	0.2071	38
PbSe	4.305	7.715	0.2183	18
PbTe	4.568	8.019	0.2298	6

[a]Results from LDA in Ref. [40]

To study the dynamic stabilities of PbS in this nonpolar structure, we have calculated the phonon spectra. The dispersion curves along high symmetry directions are plotted in Fig. 1(c). We can find that the nonpolar phase exhibits imaginary phonon frequencies (negative values) along the Γ-K direction, explicitly showing an TO mode with an imaginary frequency of 63 cm^{-1} at the BZ center (Γ point). This soft phonon mode is polarized along the z direction with the displacement eigenvector of $[\delta(\text{Pb}) = +0.018, \delta(\text{S}) = -0.165]$, which corresponds to vibrations in the [0001] direction. It is evident that the $P6_3/mmc$ PbS is dynamically unstable. It is possible for the S atoms to displace along the direction of the soft mode, converting the nonpolar phase into a dynamically stable structure, as sketched in Fig. 1(d). The resulting polar phase is in the distorted NiAs-type structure with the space group $P6_3mc$. In this polar structure, the Pb atoms are in Wyckoff position 2a (0, 0, 0) and the S atom in 2b (1/3, 2/3, z). The soft phonon mode (with an imaginary frequency) in the nonpolar phase is energetically favorable to drive the ferroelectric phase transition, from the nonpolar high-symmetry reference phase with the $P6_3/mmc$ symmetry into a polar $P6_3mc$ phase.

The optimized structural parameters of polar PbS in the polar $P6_3mc$ phase are given in Table I. The previous LDA results are also given for comparison. We confirmed that there are no imaginary phonon frequencies in the $P6_3mc$ phase (see Fig. S2 in the Supplemental Material [41]). The calculated polarization is 0.42 C/m^2, which is comparable to the polarization of the typical ferroelectrics such as $BaTiO_3$ and hexagonal ABC in the LiGaGe-type structure [6]. We have calculated the energy difference between the polar $P6_3mc$ phase and the nonpolar $P6_3/mmc$ phase to appraise the switchability of the polarization. Such energy barrier characterizes the uniform switching of the polarization and can be used to estimate the barrier for realistic switching [6]. The energy barrier is calculated to be 0.038 eV. In comparison, the values for $BaTiO_3$ and $PbTiO_3$ are 0.02 and 0.2 eV, respectively, showing that the barrier in PbS is sufficiently small for switching. In addition, the calculated coercive electric field is about 1.95 kV/cm using the Landau theory [41], which indicates the possibility to switch the spontaneous polarization by a small external electric filed. Thus, PbS in the distorted NiAs-type structure can be a candidate of ferroelectricity.

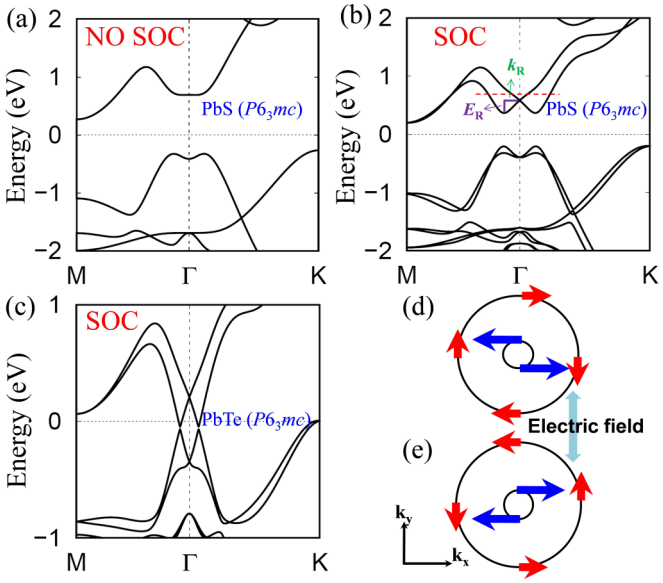

FIG. 2. Electronic band structures of polar PbS ($P6_3mc$) along the high-symmetry directions of the Brillouin zone calculated (a) without SOC and (b) with SOC. Rashba type spin-splitting can be found near Γ. Rashba energy E_R and the momentum offset k_R are also shown. (c) Electronic band structures of polar PbTe ($P6_3mc$) calculated with SOC. (d, e) The spin texture of the conduction bands at 0.65 eV [dashed line in (b)] for polar PbS. With the switching of the ferroelectric polarization by external electric field, the spin texture is reversed.

By making use of the ferroelectricity, interesting possible applications are nonvolatile memories and ferroelectric tunnel junctions based memories. The distortion in polar PbS can also be understood in the framework of *active* lone pairs [15] as can be verified in Fig. S3(b) in the Supplemental Material [41], where asymmetric electron density distributions around Pb are found.

Figure 2(a) shows the electronic band structure of the polar PbS calculated without SOC. The band gap at the Γ point is about 1.1 eV. For the $P6_3mc$ symmetry, the group of the wave vector $\boldsymbol{k}$ at the BZ center is C_{6v}. Hence, all states at the Γ point could transform according to one of the single-group representations of C_{6v}. In this case, the mixing between states with atomic-like s and p_z character is allowed [42]. Such mixing state belongs to the Γ_1 representation. We find that both the valence band maximum (VBM) and the conduction band minimum (CBM) at the Γ point have the same Γ_1 symmetry.

When spin-orbit interaction is considered, then the states transform according to the double-group representations. In specific, Γ_1 now transforms to Γ_7. As a result, both VBM and CBM transform according to the Γ_7 representation. Thus, our system fulfils all the three criteria for the giant Rashba effects acquisition: the narrow band gap, the same symmetry character for VBM and CBM, and strong spin-orbit coupling (SOC) [43]. On the other hand, the linear term of the effective spin-splitting Hamiltonian is $H \sim (\sigma_x k_x - \sigma_y k_y)$ for the C_{6v} symmetry, because both (σ_x, σ_y) and (k_x, k_y) belong to the Γ_5 representation [42]. This is a typical Rashba-type Hamiltonian. From these above analyses, a giant Rashba effect in polar PbS with the $P6_3mc$ symmetry is highly expected. The Rashba

TABLE II. The Rashba energy splitting (E_R), the momentum offset (k_R), and the Rashba coefficient (α_R) in the valence and conduction bands along the Γ-M direction for polar PbX (X = S, Se, and Te) in the distorted NiAs-type structure.

	Valence band			Conduction band		
	E_R (meV)	k_R ($1/\text{Å}^{-1}$)	α_R (eV Å)	E_R (meV)	k_R ($1/\text{Å}^{-1}$)	α_R (eV Å)
PbS	186	0.122	3.04	218	0.120	3.63
PbSe	322	0.109	5.90	304	0.109	5.57
PbTe	275	0.065	8.46	250	0.065	7.69

effect can be characterized by three parameters: the Rashba energy E_R, the momentum offset k_R, and the Rashba parameter α_R, where k_R is the momentum offset between VBM (or CBM) and the energy degeneracy point [the high symmetry points, such as the Γ point in Fig. 2(b)], E_R is the difference between band energy values at k_R and at the degeneracy point, and $\alpha_R = 2E_R/k_R$ in the nearly free electron approximation [44].

Figure 2(b) displays the electronic band structure calculated with SOC, in which k_R and E_R are indicated, with lifted band degeneracy observed. Bands near the Γ point typify a clear Rashba split band structure. Note that two branches in the conduction band follow linear dispersion around Γ, which in turn form a Dirac cone [45]. Accordingly, we obtain $k_R = 0.120\,\text{Å}^{-1}$ and $E_R = 218$ meV in the conduction band along the Γ-M direction, and the corresponding Rashba parameter α_R is 3.63 eV Å. Moreover, one can also find analogical Dirac-like state in the valence band. However, the Dirac cone in the valence band is heavily deformed. The Rashba parameter of the valence band is 3.04 eV Å as listed in Table II. The spin-texture reveals the characteristic of the spin splitting, which can be obtained by computing the expectation value of the spin operators. The spin-textures of the inner and outer branches of the conduction band near the Γ point are shown in Fig. 2(d). Note that the spin is always perpendicular to the momentum due to spin-momentum locking. The inner and outer bands have counterclockwise and clockwise spin textures, respectively. With the switching of the ferroelectric polarization, the spin texture reversed, as indicated in Fig. 2(e). This provides a means to control the spin polarization by the electric field. Based on this property we can design a generation of spintronic devices, such as Datta-Das spin transistors with Rashba ferroelectrics as the channel.

As presented in Table I, two polar phases PbSe and PbTe have even lower energy berries than that of PbS. The corresponding Rashba related parameters are given in Table II. The Rashba parameters α_R for PbSe and PbTe are 5.9 and 8.46 eV Å, which are much larger than the previously reported values of 4.8, 1.82, and 0.74 eV Å for GeTe [18], LiZnSb [46], and $BiAlO_3$ ($P4mm$) [44], respectively. The electronic band structures of the polar phase PbTe calculated with SOC are shown in Fig. 2(c). The energy bands near the Γ point display a Rashba-type character with Dirac cones. The Fermi level crosses the conduction band near the Γ point, indicating a semimetallic ferroelectric. The above investigations can be straightforwardly generalized to other IV-VI compounds. The

TABLE III. Theoretical results for polar IV-VI compounds in the distorted NiAs-type structure. z is the position (in fractional coordinates) of anion in the z direction (c axis). ΔE is the energy difference (calculated with SOC) between the polar state ($P6_3mc$) and the nonpolar reference state ($P6_3/mmc$).

	a (Å)	c (Å)	z	ΔE (meV)
SnS	3.941	8.188	0.1770	161
SnSe	4.141	8.042	0.1929	80
SnTe	4.416	8.182	0.2089	27
GeS	3.530	9.524	0.1419	389
GeSe	3.830	8.091	0.1741	228
GeTe	4.125	8.059	0.1896	118

structural parameters and energy barriers for these lead-free polar IV-VI phases are collected in Table III. We find that both polar SnTe and GeTe are semimetals as can be found from the band structures shown in Fig. S4 in the Supplemental Material [41]. Thus, they are Rashba ferroelectric semimetals, which can be experimentally realized since ferroelectric transitions in metals have already been reported [17]. In addition to these compounds, ferroelectrics may also be discovered in compounds containing other group elements in the NiAs-type structure, possibly with the assistance of strain engineering [47].

B. Topological surface states and type-II Dirac points

Nontrivial electronic characters also take place in the nonpolar phases of these compounds. Specifically, the band structures of nonpolar PbSe are shown in Fig. 3. Figure 3(a) shows the band structure calculated without SOC. Near the Γ point, there exist band crosses between the conduction band (Pb p_z orbital character) and the valence band (Se p_z orbital character). This is a band inversion with a negative energy gap at the Γ point. Different from Bi_2Se_3, the existence of the band inversion in PbSe is not due to the presence of SOC. Once SOC is taken into account, a band gap is then opened up at the band crossing points, as shown in Fig. 3(b). For space group $P6_3/mmc$, the little group of k-points along the Γ-M line, i.e., Σ(u, 0, 0) point, is C_{2v}. There is only one irreducible representation Σ_5 for the double group C_{2v} [48]. The band crossing between the conduction band and valence band along the Γ-M line is forbidden since they both belong to the Σ_5 representation. Thus, SOC opens a gap. One the other hand, the little group of k-points along the Γ-K line, i.e. Λ(u, u, 0) point, is also C_{2v}. A band gap is then also opened up at the band crossing point for the same reason. The gap is about 0.41 eV at the Γ point. Thus, SOC plays a very different role in PbSe, and HgTe (Bi_2Se_3). The nonpolar PbSe is a topologically nontrivial phase with Z_2 topological invariants (1;000) [41]. To further understand the topological properties, we have calculated the surface band structures in the (0001) hexagonal surface BZ. In Fig. 3(c) we show the nontrivial surface states [39] for the Se terminated surface, which have linear dispersions and form a Dirac cone, connecting the bulk conduction states and bulk valence states. The Dirac point is buried in the bulk states. The topological states belong to a class which is invariant under TR symmetry. As long as the TR symmetry is preserved, the metallic topological surface states cannot be gapped out. For the Pb terminated surface, a clearer Dirac cone appears within the bulk gap as shown in Fig. 3(d). This indicates a termination dependent character of the topological states. To check the validity of our PBE results, we have also considered the HSE functional [36]. The surface states calculated with HSE functional, illustrated in Fig. S5(b) and Fig. S5(c) in the Supplemental Material [41], show no significant difference, in line with the PBE results. Materials with topological surface states have potential technological applications, such as robust spintronic devices and transistors with low power dissipation.

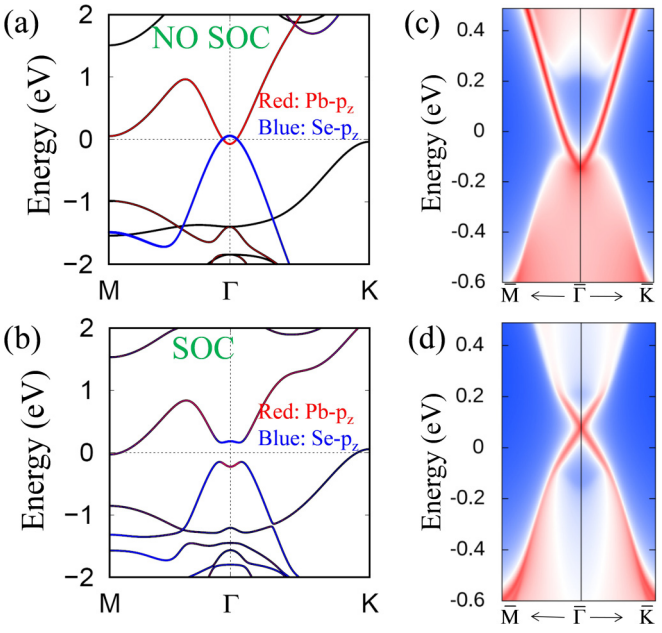

FIG. 3. Electronic band structures of nonpolar high-symmetry PbSe ($P6_3/mmc$) calculated (a) without SOC and (b) with SOC. The color lines indicate the projection to the Pb p_z (red) and Se p_z (blue) states. Surface spectral functions for the (c) Se-terminated and (d) Pb-terminated (0001) hexagonal surfaces.

Figure 4 shows the band structure along the Γ-A line [see Fig. 1(b) for the details of BZ], with the inclusion of SOC for PbTe (with the nonpolar $P6_3/mmc$ symmetry). There exists band crossing between two low-lying valence bands. The little group of k points along the Γ-A line, i.e., Δ(0, 0, u) point, is C_{6v}. According to the double-group representations, the two bands transform according to two different representations. Therefore, the band crossing is inevitable, protected by crystal symmetry. The band dispersion is linear around each node, which results in a pair of strongly tilted type-II Dirac cones that are located at $\boldsymbol{k}_c = (0,0,\pm 0.338)$ (in units of $Å^{-1}$) along the Γ-A line.

C. Synthesis feasibility

The final issue to be discussed is the synthesis feasibility of these compounds in the distorted NiAs-type structure, which is experimentally unknown up to now. The distorted NiAs-type structure was reported by Zagorac *et al.* as a result of a global structural search on the energy landscape of PbS [40]. PbS in the undistorted NiAs-type structure was also predicted in

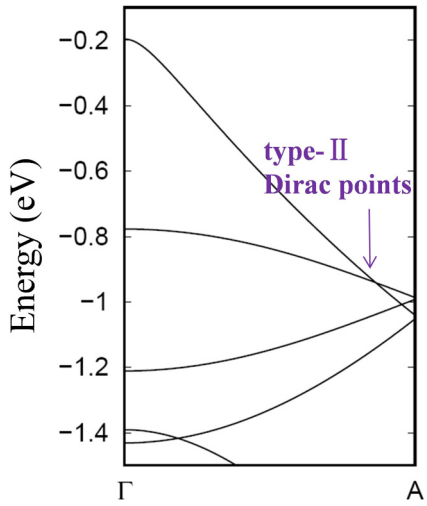

FIG. 4. Electronic band structures of nonpolar high-symmetry PbTe ($P6_3/mmc$) calculated with SOC. The arrow indicates the type-II Dirac points.

the same work [40]. The ground state of PbS has NaCl-type structure ($Fm\text{-}3m$). We have given the energy-volume curves for three phases in Fig. S7 in the Supplemental Material [41]. The energy of the $P6_3mc$ phase is only 0.11 eV per formula unit higher than that of the $Fm\text{-}3m$ phase. The advanced epitaxial growth techniques, which can provide possible pathway to grow structures that are inaccessible by traditional means, may provide opportunities to synthesize this class of ferroelectrics with simple crystal structures.

IV. CONCLUSIONS

In summary, we have predicted a class of diatomic ferroelectrics in the distorted NiAs-type structure using first-principles methods. The ferroelectric well depths are sufficiently small to switch the ferroelectric polarization experimentally. In addition to Rashba ferroelectric semiconductors (polar PbS and PbSe), Rashba ferroelectric semimetals (e.g., polar PbTe, SnTe, and GeTe) are found. Topological surface states (nonpolar PbSe) and type-II bulk Dirac fermions (in nonpolar PbTe) are predicted. Rich physical properties in this class of materials deserve further theoretical and experimental investigations. These multifunctional materials have wide technological applications prospects in spin-orbitronics devices.

ACKNOWLEDGMENTS

This work was supported by National key research and development program (Grant No. 2016YFB0901600), the NSF of China under Grants No. 11474145, No. 11334003, and No. 21573117, and the special Program for Applied Research on Super Computation of the NSFC-Guangdong Joint Fund (the second phase) under Grant No. U1501501.

[1] R. Resta, Rev. Mod. Phys. **66**, 899 (1994).
[2] K. Rabe, C. H. Ahn, and J.-M. Triscone, *Physics of Ferroelectrics: A Modern Approach* (Springer, New York, 2007).
[3] V. Garcia, M. Bibes, L. Bocher, S. Valencia, F. Kronast, A. Crassous, X. Moya, S. Enouz-Vedrenne, A. Gloter, D. Imhoff, C. Deranlot, N. D. Mathur, S. Fusil, K. Bouzehouane, and A. Barthelemy, Science **327**, 1106 (2010).
[4] J. F. Scott, Science **315**, 954 (2007).
[5] J. Valasek, Phys. Rev. **17**, 475 (1921).
[6] J. W. Bennett, K. F. Garrity, K. M. Rabe, and D. Vanderbilt, Phys. Rev. Lett. **109**, 167602 (2012).
[7] R. Fei, W. Kang, and L. Yang, Phys. Rev. Lett. **117**, 097601 (2016).
[8] W. Ding, J. Zhu, Z. Wang, Y. Gao, D. Xiao, Y. Gu, Z. Zhang, and W. Zhu, Nat. Commun. **8**, 14956 (2017).
[9] D. Di Sante, A. Stroppa, P. Barone, M.-H. Whangbo, and S. Picozzi, Phys. Rev. B **91**, 161401(R) (2015).
[10] L. Seixas, A. S. Rodin, A. Carvalho, and A. H. Castro Neto, Phys. Rev. Lett. **116**, 206803 (2016).
[11] P. Z. Hanakata, A. S. Rodin, A. Carvalho, H. S. Park, D. K. Campbell, and A. H. Castro Neto, Phys. Rev. B **96**, 161401(R) (2017).
[12] E. Bruyer, D. Di Sante, P. Barone, A. Stroppa, M.-H. Whangbo, and S. Picozzi, Phys. Rev. B **94**, 195402 (2016).
[13] G. S. Pawley, W. Cochran, R. A. Cowley, and G. Dolling, Phys. Rev. Lett. **17**, 753 (1966).
[14] D. Yang, T. Chatterji, J. A. Schiemer, and M. A. Carpenter, Phys. Rev. B **93**, 144109 (2016).
[15] D. J. Payne, R. G. Egdell, A. Walsh, G. W. Watson, J. Guo, P. A. Glans, T. Learmonth, and K. E. Smith, Phys. Rev. Lett. **96**, 157403 (2006).
[16] P. W. Anderson and E. I. Blount, Phys. Rev. Lett. **14**, 217 (1965).
[17] Y. Shi, Y. Guo, X. Wang, A. J. Princep, D. Khalyavin, P. Manuel, Y. Michiue, A. Sato, K. Tsuda, S. Yu, M. Arai, Y. Shirako, M. Akaogi, N. Wang, K. Yamaura, and A. T. Boothroyd, Nat. Mater. **12**, 1024 (2013).
[18] D. Di Sante, P. Barone, R. Bertacco, and S. Picozzi, Adv. Mater. **25**, 509 (2013).
[19] S. Datta and B. Das, Appl. Phys. Lett. **56**, 665 (1990).
[20] M. Z. Hasan and C. L. Kane, Rev. Mod. Phys. **82**, 3045 (2010).
[21] X.-L. Qi and S.-C. Zhang, Rev. Mod. Phys. **83**, 1057 (2011).
[22] A. Bansil, H. Lin, and T. Das, Rev. Mod. Phys. **88**, 021004 (2016).
[23] H. Huang, S. Zhou, and W. Duan, Phys. Rev. B **94**, 121117(R) (2016).
[24] T.-R. Chang, S.-Y. Xu, D. S. Sanchez, S.-M. Huang, G. Chang, C.-H. Hsu, G. Bian, I. Belopolski, Z.-M. Yu, X. Xu, C. Xiang, S. A. Yang, T. Neupert, H.-T. Jeng, H. Lin, and H. M., arXiv:1606.07555.
[25] C. Le, S. Qin, X. Wu, X. Dai, P. Fu, C. Fang, and J. Hu, Phys. Rev. B **96**, 115121 (2017).
[26] M. Yan, H. Huang, K. Zhang, E. Wang, W. Yao, K. Deng, G. Wan, H. Zhang, M. Arita, H. Yang, Z. Sun, H. Yao, Y. Wu, S. Fan, W. Duan, and S. Zhou, Nat. Commun. **8**, 257 (2017).
[27] D. Di Sante, P. Barone, A. Stroppa, K. F. Garrity, D. Vanderbilt, and S. Picozzi, Phys. Rev. Lett. **117**, 076401 (2016).

[28] R. O. Jones, Rev. Mod. Phys. **87**, 897 (2015).
[29] J. P. Perdew, K. Burke, and M. Ernzerhof, Phys. Rev. Lett. **77**, 3865 (1996).
[30] G. Kresse and J. Furthmuller, Phys. Rev. B **54**, 11169 (1996).
[31] M. Gajdoš, K. Hummer, G. Kresse, J. Furthmüller, and F. Bechstedt, Phys. Rev. B **73**, 045112 (2006).
[32] J. Hafner, J. Comput. Chem. **29**, 2044 (2008).
[33] H. J. Monkhorst and J. D. Pack, Phys. Rev. B **13**, 5188 (1976).
[34] R. D. King-Smith and D. Vanderbilt, Phys. Rev. B **47**, 1651 (1993).
[35] A. Togo and I. Tanaka, Scripta Mater. **108**, 1 (2015).
[36] J. Heyd, G. E. Scuseria, and M. Ernzerhof, J. Chem. Phys. **118**, 8207 (2003).
[37] A. A. Mostofi, J. R. Yates, Y.-S. Lee, I. Souza, D. Vanderbilt, and N. Marzari, Comput. Phys. Commun. **178**, 685 (2008).
[38] A. A. Mostofi, J. R. Yates, G. Pizzi, Y.-S. Lee, I. Souza, D. Vanderbilt, and N. Marzari, Comput. Phys. Commun. **185**, 2309 (2014).
[39] Q. S. Wu, S. N. Zhang, H.-F. Song, M. Troyer, and A. A. Soluyanov, arXiv:1703.07789.
[40] D. Zagorac, K. Doll, J. C. Schön, and M. Jansen, Phys. Rev. B **84**, 045206 (2011).
[41] See Supplemental Material at http://link.aps.org/supplemental/10.1103/PhysRevB.96.245136 for details about computational details and other materials.
[42] L. C. Lew Yan Voon, M. Willatzen, M. Cardona, and N. E. Christensen, Phys. Rev. B **53**, 10703 (1996).
[43] M. S. Bahramy, R. Arita, and N. Nagaosa, Phys. Rev. B **84**, 041202(R) (2011).
[44] L. G. D. da Silveira, P. Barone, and S. Picozzi, Phys. Rev. B **93**, 245159 (2016).
[45] H. Murakawa, M. S. Bahramy, M. Tokunaga, Y. Kohama, C. Bell, Y. Kaneko, N. Nagaosa, H. Y. Hwang, and Y. Tokura, Science **342**, 1490 (2013).
[46] A. Narayan, Phys. Rev. B **92**, 220101(R) (2015).
[47] K. J. Choi, M. Biegalski, Y. L. Li, A. Sharan, J. Schubert, R. Uecker, P. Reiche, Y. B. Chen, X. Q. Pan, V. Gopalan, L. Q. Chen, D. G. Schlom, and C. B. Eom, Science **306**, 1005 (2004).
[48] http://www.cryst.ehu.es/.